A THREE-DIMENSIONAL FVC SCHEME ON NON-UNIFORM TETRAHEDRON MESHES: APPLICATION TO THE 3D-EULER EQUATIONS

M. ZIGGAF[1,2,3], **I. KISSAMI**[2], **M. BOUBEKEUR**[3], **I. ELMAHI**[1,2], **F. BENKHALDOUN**[3]

[1]ENSAO, Mohamed 1st University Complexe Universitaire, B.P. 669, 60000 Oujda, Morocco
e-mail: Moussa.ZIGGAF@um6p.ma   ziggaf@math.univ-paris13.fr

[2]MSDA, Mohammed VI Polytechnic University Lot 660, 43150 Ben Guerir, Morocco email:
Imad.KISSAMI@um6p.ma, Imad.ELMAHI@um6p.ma

[3]Sorbonne Paris North University, LAGA, CNRS, UMR 7539, F-93430, Villetaneuse, France
email: fayssal@math.univ-paris13.fr, boubekeur@math.univ-paris13.fr

Key words: FVC Scheme, Euler equations, Spacetime Discretization, Characteristics Curves.

Abstract. This study is about the construction of a numerical scheme of the predictor-corrector type in conservative form for solving general systems of conservation laws in multiple space dimensions on unstructured meshes. The work is a generalization of the one-dimensional finite volume characteristics (FVC) scheme and is related to the work of Fayssal Benkhaldoun and Mohammed Sead. The construction of the intermediate state is based on the method of characteristics, while the corrective stage recovers the conservation equations. The scheme is accurate to first order, monotonic and entropic; it avoids Riemann solvers at each interface; it also allows for improved accuracy order in time and space on unstructured three-dimensional meshes in the framework of the finite volume method. The scheme's performance is evaluated through a series of test benchmarks for the three-dimensional version of the Euler equations..

1 INTRODUCTION

A complementary approach for experiment and modeling, numerical simulation is one of the three pillars of scientific research. Fluid mechanics is one of the pioneering sectors in this triptych, and obtaining numerical schemes well suited to fluid mechanics models is a subject that has occupied numerical scientists for some time. One of the difficulties is to reconcile accuracy and robustness with a reasonable computational cost, but the complications can be quite different depending on the applications targeted. Thus, despite the numerous works and the advances in a subject that is still relevant today, it is quite natural that there is no uniformly efficient technique in all regimes. In the context of the numerical approximation of hyperbolic systems of conservation laws, several methods based essentially on the solution of the Riemann problem have been retained, and concern shock capture schemes [7, 8, 9, 10]. These methods propose schemes allowing the exact solution of the Riemann problem on each interface, which makes their computation algorithm very expensive. To reduce the computational time, other approaches propose an approximate solution to the Riemann problem, and for the same purpose,

the work of Roe [4, 5] and Hartan [6] provided a scheme based on the evaluation of numerical flux from the exact solution of the linearized problem, the industry widely uses this scheme because it has the ability to capture shock waves with reasonable accuracy.

This paper aims to describe a simple approach that may be a good candidate for the simulation of most compressible flow phenomena in real configurations. The proposed approach is a new family of numerical schemes that incorporates the techniques of the method of characteristics in the reconstruction of numerical flux, it is easy to implement, and it accurately solves hyperbolic systems of conservation laws; it is also written in the formalism of non-uniform tetrahedral meshes, in addition, this scheme avoids the resolution of Riemann problem in the time integration process, it is conservative and can be considered as a finite volume method without a Riemann solver for the Euler equations. To approximate the characteristic curves, an iterative process is used, and the numerical fluxes are calculated using interpolation. Let us mention that the advantage of using the characteristic method is that no boundary conditions are necessary for the numerical flows at the predictor stage. These features are demonstrated using several reference problems for the Euler equations. The results presented provide accurate and efficient solutions. In this paper, the reader will find a process that will allow him to have a programmable solution and be capable of generating the numerical solutions of Euler equations for incompressible flows.

This paper is structured as follows: a brief description of the mathematical model and the predictor-corrector algorithm of the multidimensional FVC scheme will be presented in Section 2. Then, numerical results and examples will be presented in Section 3. Finally, a discussion on the accuracy and efficiency of the characteristic finite volume scheme, as well as some conclusions on the paper, are disclosed in Section 4.

2   FVC scheme in multiple space dimensions

We consider the three-dimensional Euler equations modelling the dynamics of non-viscous gases

$$\partial_t \mathbf{W} + \nabla \cdot \mathbf{F}(\mathbf{W}) = 0, \tag{1}$$

with

$$\mathbf{W} = \begin{pmatrix} \rho \\ \rho u \\ \rho v \\ \rho w \\ \rho E \end{pmatrix}, \qquad \mathbf{F}(\mathbf{W}) = \begin{pmatrix} \rho u & \rho v & \rho w \\ \rho u^2 + P & \rho uv & \rho uw \\ \rho uv & \rho v^2 + P & \rho vw \\ \rho uw & \rho uw & \rho w^2 + P \\ u(\rho E + P) & v(\rho E + P) & w(\rho E + P) \end{pmatrix}. \tag{2}$$

where $\mathbf{F}$ is the flux tensor and $\mathbf{W}$ is the unknowns vector, such as ρ is the density of the gaze, $\mathbf{u} := (u, v, w)$ is the gaze particle velocity, E is the total energy, and P is pressure, knowing that the latter is related to the total energy using the law of the state of perfect gases given by

$$\rho E = (\frac{1}{2}\rho|\mathbf{u}|^2 + \frac{P}{(\gamma - 1)}) \tag{3}$$

with γ is the ratio of specific heats, it is a constant that depends on the particular gas. We formulate the three-dimensional finite volume characteristic scheme to solve the equation (1). The method uses general meshes to facilitate grid generation for complex configuration computational domains. In addition, a predictor-corrector step is used for temporal integration. In the predictor step, the method of characteristics is used to determine the intermediate values to evaluate the numerical flow, while a thoroughly conservative solution is obtained in the correction step.

2.1 FVC scheme on unstructured meshes

We assume a conforming tessellation $\mathcal{T}$ of the computational domain $\Omega \subset \mathbb{R}^3$ a by elements T_i that are called a control volume such that $\mathcal{T} = \bigcup_i T_i$.

Integrating the (1) over a control volume T_i by using Green's divergence formula, we obtain the following integral system

$$\frac{\partial}{\partial t} \int_\Omega \mathbf{W} dV + \int_{\partial\Omega} \mathbf{F}(\mathbf{W}) \cdot \mathbf{n} \ d\sigma = 0, \tag{4}$$

where Ω is the domain of interest, $\partial\Omega$ is the boundary surrounding, $\mathbf{n}$ is the normal vector to $\partial\Omega$ in the outward direction, dV and $d\sigma$ are respectively the surface element and the length element. The problem domain is first discretized into a set of triangular cells forming an unstructured computational mesh. We consider the cell-centered finite volume formulation, i.e. it starts with the discretization of the computational domain Ω by a finite set of control volumes T_i, see Figure 1, then, by integrating (1) over a control volume T_i and using Green's divergence formula, we obtain the integral system (4). A cell-centred finite volume method is formulated where all the dependent variables of the system are represented as piecewise constant in the cell. Therefore, the equation (4) can be reformulated as

$$\frac{d\mathbf{W}_i}{dt} = -\frac{1}{|T_i|} \sum_{j \in N(i)} |\gamma_{ij}| \Phi(\mathbf{W}_{ij}, \mathbf{n}_{ij}), \tag{5}$$

where $\mathbf{W}_i = \dfrac{1}{|T_i|} \displaystyle\int_{T_i} \mathbf{W} \ dV$ is the average quantity on cell T_i stored at the cell center.

$\Phi(\mathbf{W}_{ij}, \mathbf{n}_{ij}) \simeq \dfrac{1}{|\gamma_{ij}|} \displaystyle\int_{\gamma_{ij}} \mathbf{F}(\mathbf{W}) \cdot \mathbf{n}_{ij} d\sigma$, is the numerical flux computed at the interface γ_{ij} between the cells T_i and T_j. The idea of the flux approximation is to reconstruct the intermediate state $\mathbf{W}_{ij}$ as the following process.
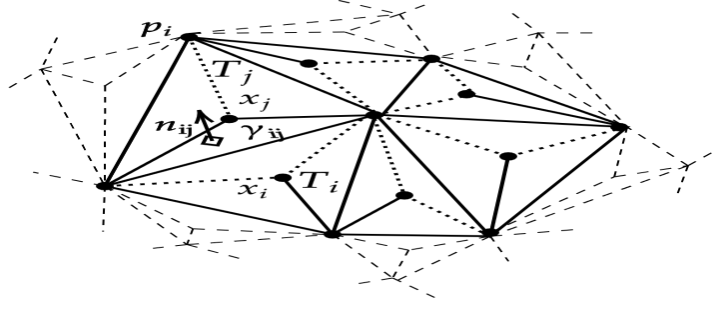
Figure 1: Generic control cells of the computational domain.

Notations:

- p_i, vertex of T_i,

- x_i, centroid of the cell T_i,

- γ_{ij}, boundary face between the cells T_i and T_j,

- $|\gamma_{ij}|$, area of γ_{ij},

- $|T_i|$, volume of the cell T_i,

- ∂T_i, boundary of the cell T_i,

- $\mathcal{P}_i$, the surface area of the cell T_i.

- $\mathbf{n}_{ij}$, unit normal to γ_{ij}, outward to T_i such as, $\mathbf{n}_{ji} = -\mathbf{n}_{ij}$.

We compute the intermediate state $\mathbf{W}_{ij}$ from a projected velocity model whose velocity components are projected onto the frame $\mathcal{R} = (\mathcal{T}_i; \vec{b}, \vec{\tau}, \vec{\eta})$ see Figure 2, where $\vec{\eta} := (n_x, n_y, n_z)^T$ is the unit outward normal to the surface of the cell T_i. $\vec{\tau} = (\tau_x, \tau_y, \tau_z)^T$ and $b = (b_x, b_y, b_z)^T$ are the tangential vectors such as, $\vec{b} := \vec{\eta} \wedge \vec{\tau}$. The projected velocities are defined as $u_\eta := \mathbf{u} \cdot \vec{\eta}$, $u_\tau := \mathbf{u} \cdot \vec{\tau}$ and $u_b := \mathbf{u} \cdot \vec{b}$, i.e.

$$\begin{pmatrix} u_\eta \\ u_\tau \\ u_b \end{pmatrix} = \begin{pmatrix} n_x & n_y & n_z \\ \tau_x & \tau_y & \tau_z \\ b_x & b_y & b_z \end{pmatrix} \cdot \begin{pmatrix} u \\ v \\ w \end{pmatrix} \tag{6}$$
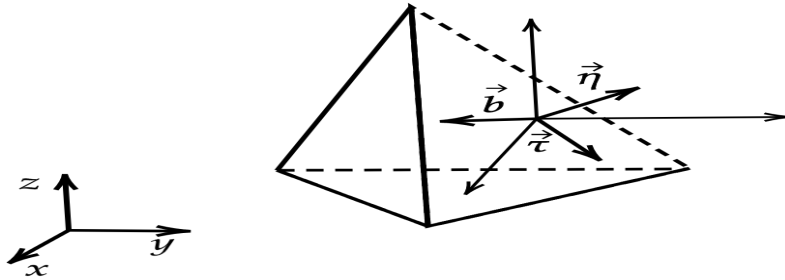
Figure 2: The projected velocity frame.

The projected speed model associated with the Euler equations (1) is reformulate

$$\frac{\partial \mathbf{U}}{\partial t}(t, X) + u_\eta(t, X) \frac{\partial \mathbf{U}}{\partial \eta}(t, X) = \mathbf{S}(\mathbf{U}), \tag{7}$$

where

$$\mathbf{U} = \begin{pmatrix} \rho \\ \rho u_\eta \\ \rho u_\tau \\ \rho u_b \\ \rho E \end{pmatrix}, \qquad \mathbf{S}(\mathbf{U}) = \begin{pmatrix} -\rho \partial_\eta(u_\eta) \\ -\rho u_\eta \partial_\eta(u_\eta) - \partial_\eta P \\ -\rho u_\tau \partial_\eta(u_\eta) \\ -\rho u_b \partial_\eta(u_\eta) \\ -\rho E \partial_\eta(u_\eta) - \partial_\eta(P u_\eta) \end{pmatrix}. \tag{8}$$

$\mathbf{U}$ is the projected conservative unknown, u_η is the normal speed, and $\mathbf{S}(\mathbf{U})$ is the second member that contains other terms of the system. The method of characteristics used traces backwards position at time t_n of particles that will reach the points of a fixed mesh at time $t_n + \alpha^n \Delta t$, $X_\star$ see Figure 3, the method avoids the grid distortion difficulties that the conventional Lagrangian schemes have. The characteristic curves associated with (7) are the solutions of the following equation

$$X(t_n) = X_\star - \int_{t_n}^{t_n + \alpha^n \Delta t} u_\eta(s, X(s)) \cdot \mathbf{n} \, ds. \tag{9}$$

In order to complete the reformulation of the algorithm used, the departure points must be calculated once the characteristic curves are known. Therefore, the solution of the advection equation (7) is

$$\mathbf{U}(t_n + \alpha^n \Delta t, X_\star) = \mathbf{U}(t_n, X(t_n)) + \int_{t_n}^{t_n + \alpha^n \Delta t} \mathbf{S}(\mathbf{U}(s, X(t_n))) \, ds. \tag{10}$$

In our implementation, we have used a global fixed value for α^n however, a local selection α_{ij}^n is also possible. The solution in the characteristic field is calculated by interpolation from cell center values.

$$\mathbf{U}_{ij}^n = \hat{\mathbf{U}}_{ij}^n + \mathbf{I_F}(\hat{\mathbf{U}}_{ij}^n), \tag{11}$$

where $\mathbf{I_F}$ is the approximation of the integral in (10) and $\hat{\mathbf{U}}_{ij}^n = \sum_{k \in V(X^c)} \beta_k(X^c) \mathbf{U}_k^n$, with $V(X^c)$ is the set of neighbours by face and vertices to the cell of X^c and $\beta_k(X^c)$ is the interpolation weight. The normal derivative terms in $\mathbf{S}$ are evaluated using the diamond scheme see [13]
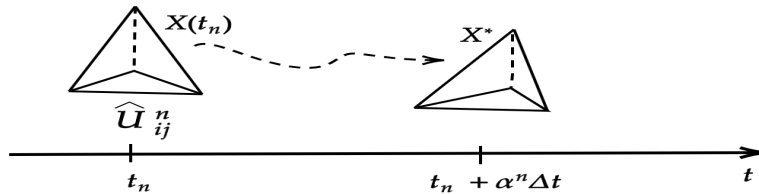
Figure 3: illustration of the time grid for the choice of the starting condition in order to calculate the characteristics of the equation (7).

One $\mathbf{U}_{ij}^n$ is calculated in the predictor step, the state $\mathbf{W}_{ij}^n$ is recovered from $\mathbf{U}_{ij}^n$ using the projection transformations (6) then, $\Phi(\mathbf{W}_{ij}^n, \mathbf{n}_{ij}) = \mathbf{F}(\mathbf{W}_{ij}^n) \cdot \mathbf{n}_{ij}$.

Regarding the temporal discretization, the equation (5) will be solved with various implicit or explicit temporal numerical schemes, amongst which are the Euler, Rung-Kutta, and Adams-Bashforth schemes. Here we have chosen the explicit Euler scheme, which is simple and fast. The time domain is divided into N sub-intervals $[t_n, \ t_{n+1}]$ with time step $\Delta t = t_{n+1} - t_n$ for $n = 0, 1, ..., N - 1$. $\mathbf{W}^n$ is the value of a generic function $\mathbf{W}$ at time t_n. The fully-discrete formulation of the equation (4) is given by

$$\mathbf{W}_i^{n+1} = \mathbf{W}_i^n - \frac{\Delta t}{|T_i|} \sum_{j \in N(i)} |\gamma_{ij}| \Phi(\mathbf{W}_{ij}^n, \mathbf{n}_{ij}). \tag{12}$$

For the systems of conservation laws, such as the compressible Euler equations, all of the reconstruction procedures are implemented in the characteristic local directions to avoid spurious oscillations.

3 Numerical results

In this study, the Courant-Friedrichs-Lewy number for the explicit scheme (12) can be written under the following condition

$$\Delta t \leqslant \min \left\{ \frac{|T_i|}{\mathcal{P}_i(|\mathbf{u} \cdot \mathbf{n}| + \sqrt{\gamma P / \rho})}, \frac{|T_i|}{\mathcal{P}_i(|\mathbf{u} \cdot \mathbf{n}| + \sqrt{\gamma P / \rho}) \sqrt{2\alpha^n}} \right\},$$ see [14]. A fixed CFL = 0.9 is used and $\alpha^n = 1$ for first order approximation. Specific heat ratio $\gamma = 1.4$ is expected.

3.1 Shock tube problem

We consider a tube of length $1m$, separated in the middle by a membrane with on one side a gas at high pressure (p_l, ρ_l) and on the other a gas at low pressure (p_r, ρ_r). Due to the pressure difference. A shock wave propagates in the low-pressure chamber, followed by a contact discontinuity, and an expansion wave propagates in the high-pressure chamber. Note that the contact discontinuity is only visible on the density. The initial conditions are given by

$$(\rho, p, u)(0, x, y, z) = \begin{cases} (\rho_l, p_l, u_l) & if \ x \leqslant x_m, \\ (\rho_r, p_r, u_r) & if \ x > x_m, \end{cases} \quad 0 \leqslant x \leqslant 1, \quad 0 \leqslant y \leqslant 0.04, \quad 0 \leqslant z \leqslant 0.04$$

$$v(0, x, y, z) = w(0, x, y, z) = 0 \ m/s.$$

Table 1: Initial states left and right and simulation end times for the 3D shock-tube problem.

Test case	ρ_l	u_l	p_l	ρ_r	u_r	p_r	t_{end}
1	1.0	0.0	10.0	0.125	0.0	1.0	0.06
2	0.445	0.698	3.528	0.5	0.0	0.571	0.14
3	1.0	-2.0	0.4	1.0	2.0	0.4	0.15

The mesh used is a non-uniform tetrahedron grid of 22626 cells and 5846 nodes, the results obtained are displayed at time *tend* given in Table 1. We present in the Figure 7 the cross-section

at $(y = 0.02m, z = 0.02m)$ of the density and the pressure for each test case of the Table 1. For a better comparison, we also include the exact solution to the shock tube problem, as it can be seen that the contact discontinuity and the shock wave are very well captured and that the FVC scheme can generate its results with accuracy. It should be noted that the performance of the FVC method is very interesting for shallow water equations, see [12].
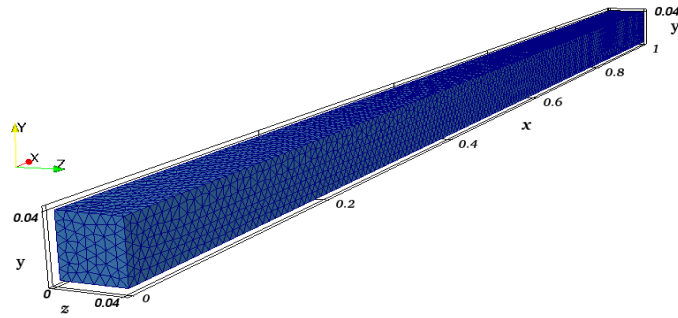
Figure 4: Unstructured tetrahedral mesh used for the 3D shock tube problems.
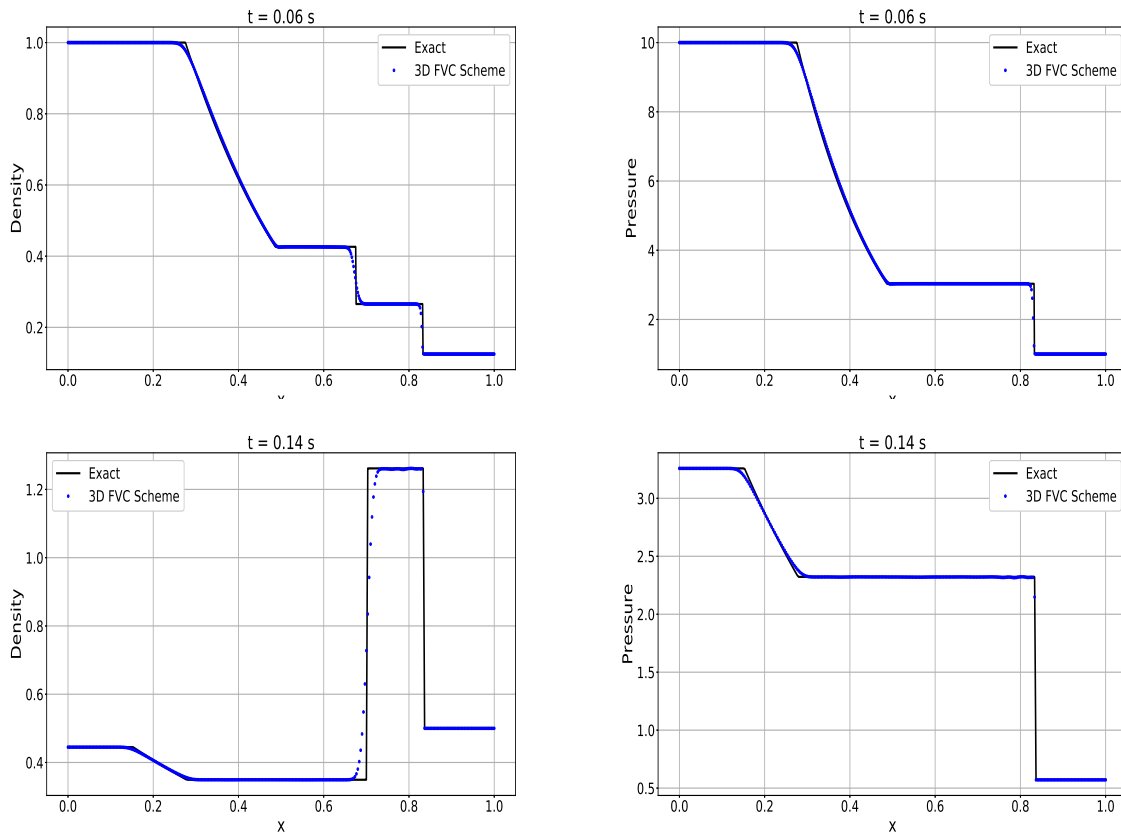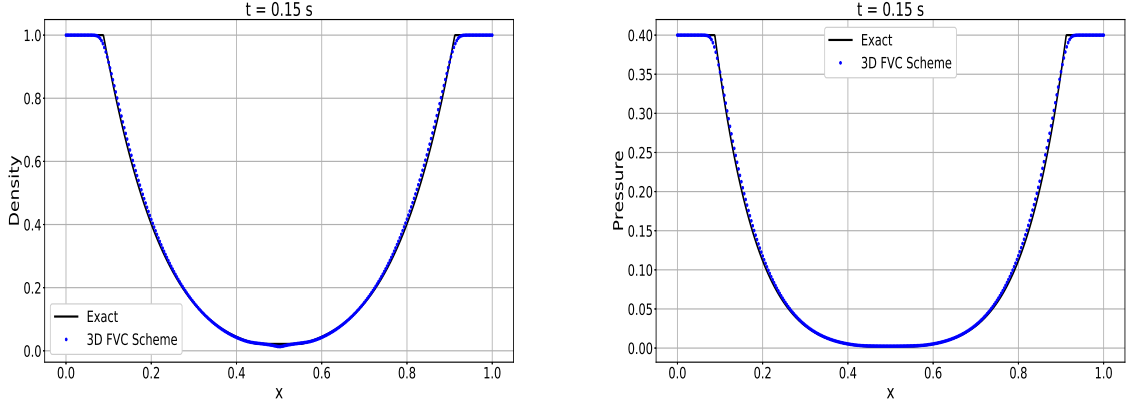
Figure 7: A cross-section at $(y = 0.02m, z = 0.02m)$ of the numerical solution of a shock tube problem in comparison with the exact solution. All figures show that the numerical solution agrees with the exact solution. We notice a small numerical diffusion which will be adjusted with the increase in order in time and space.

We show in Table 2 below an excellent agreement obtained between the numerical and analytical results, such as the L^1 error and the accuracy order of ρ and P are presented, respectively. The comparison shows that, under this condition, our scheme can accurately predict the shock wave without creating oscillations.

Table 2: Relative L^1 error and CPU times for test 1 [15] using FVC scheme with $\alpha = 1.5$.

# Cells	Maximum of cells height size	Error in ρ	Error in P	Order	CPU time (s)
4141	0.0143	1.878E-04	1.739E-04	-	4.82
11546	0.00812	1.034E-04	1.001E-04	1.311	8.32
23567	0.00645	4.518E-05	3.711E-05	1.356	18.36
43985	0.003679	1.986E-05	1.138E-05	1.409	23.34

In this work, we have developed a code manapy [16] this code is based on the solution of the Euler equations using the FVC scheme in unstructured meshes. The CFL is fixed at 0.8 and the used computer is an Intel Core i7-8565U CPU @ 1.80GHz × 8, with 15 GB RAM.
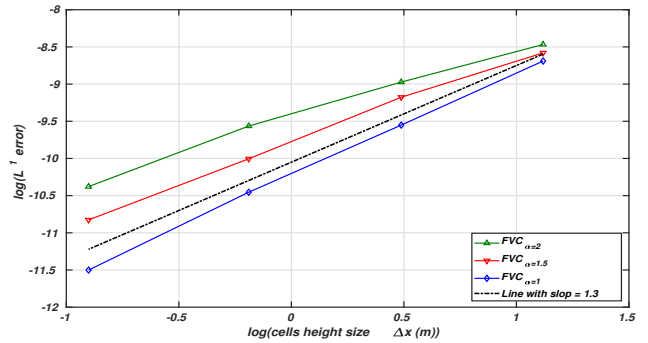
Convergence order in L^1 error of a density.

3.2 3D GAMM channel

This example was proposed in its two-dimensional version in [11] to study the subsonic and transonic flows described by the Euler equations in a channel. The flow in the channel is initially uniform and then the flow tangency condition for the walls and non-reflective condition for both upstream and downstream the Dirichlet boundaries are applied.

The solution domain is a cube $[0, 3] \times [0, 1] \times [0, 0.5]$ with a circular bump of height 10% on the lower side see Figure 8. The initial conditions are: $\rho = 1$ in the whole domain and $P = \frac{1}{\gamma}$. The output boundary $P = 0.736952$. The rest of the boundary is a non-permeable wall, so we prescribe a normal velocity component equal to zero. The figures show the numerical results generated by FVC scheme.
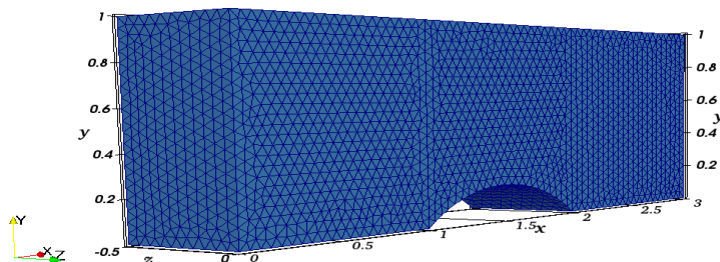
Figure 8: Computation mesh with 53065 cells for the channel flow with a 10% thick circular arc bump.
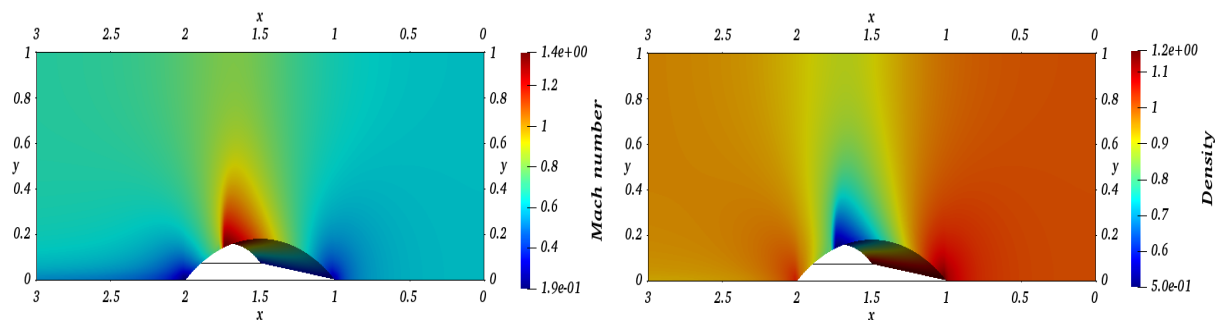
Figure 9: Mach number (left) and Density (right) at time t which is assumed to be an equilibrium time.

9
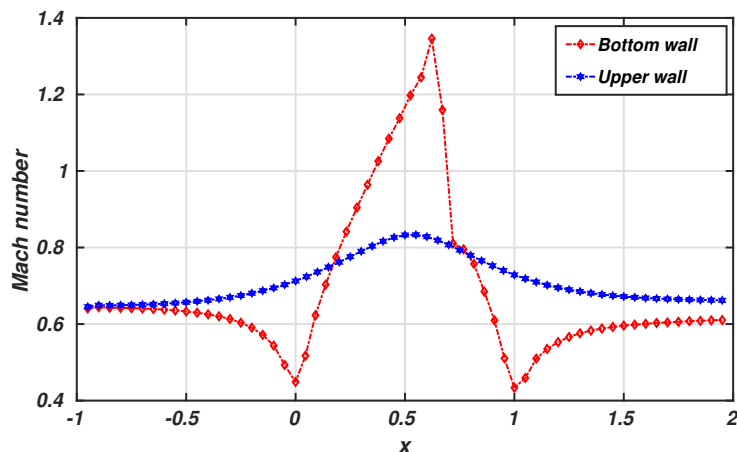
Figure 10: Mach number on bottom and upper wall $M_{max} = 1.3891$

The figures of Figure 9 shows the Mach number distribution and density of the steady-state solution. As shown in Figure 9, the numerical solution is fairly symmetrical concerning the median chord which is a good indication of the accuracy of the solution for this subsonic application. According to the calculation, a supersonic region appears in the solution which ends with a shock as shown in Figure 10 (Inviscid compressible flow in the GAMM channel: and Mach number on bottom and upper wall).

4   Concluding remarks

A generalization of the one-dimensional FVC scheme to multiple space dimensions for solving the Euler equations on general meshes in two regimes, stationary and unsteady, has been presented. Furthermore, the first results of the internal transonic flow problems obtained by the Finite Volume Characteristic scheme are presented. The agreement between the numerical results and the analytical solution for the unsteady flow case (Shock tube problem) is good and promising. The results obtained for the GAMM channel satisfy both the maximum Mach number parameters and the ability to generate steady states with acceptable accuracy. The approach has several advantages. First, it can solve stationary flows without large numerical errors, thus demonstrating that the proposed scheme achieves numerical results. Second, it can calculate the numerical flow corresponding to the actual state of the gas flow without relying on Riemann problem solvers. Furthermore, it has strong applicability to various hyperbolic conservation law models, as shown by its formulation. Future work aims at extending the presented method for the solution of incompressible Navier-Stokes equations.

REFERENCES

[1] Lee, B. J., Toro, E. F., Castro, C. E., & Nikiforakis, N. (2013). Adaptive Osher-type scheme for the Euler equations with highly nonlinear equations of state. Journal of Computational Physics, 246, 165-183.

[2] Colella, P., & Glaz, H. M. (1985). Efficient solution algorithms for the Riemann problem for real gases. Journal of Computational Physics, 59(2), 264-289.

[3] Toro, E. F., Castro, C. E., & Lee, B. J. (2015). A novel numerical flux for the 3D Euler equations with general equation of state. Journal of Computational Physics, 303, 80-94.

[4] Roe, P. L. (1981). Approximate Riemann solvers, parameter vectors, and difference schemes. Journal of computational physics, 43(2), 357-372.

[5] Roe, P. L. (1986). Characteristic-based schemes for the Euler equations. Annual review of fluid mechanics, 18(1), 337-365.

[6] Harten, A. (1997). High resolution schemes for hyperbolic conservation laws. Journal of computational physics, 135(2), 260-278.

[7] Baldauf, M. (2021). A horizontally explicit, vertically implicit (HEVI) discontinuous Galerkin scheme for the 2-dimensional Euler and Navier-Stokes equations using terrain-following coordinates. Journal of Computational Physics, 446, 110635.

[8] Abgrall, R., Bacigaluppi, P., & Tokareva, S. (2019). High-order residual distribution scheme for the time-dependent Euler equations of fluid dynamics. Computers & Mathematics with Applications, 78(2), 274-297.

[9] Varma, D., & Chandrashekar, P. (2019). A second-order, discretely well-balanced finite volume scheme for Euler equations with gravity. Computers & Fluids, 181, 292-313.

[10] Halama, J., Arts, T., & Fořt, J. (2004). Numerical solution of steady and unsteady transonic flow in turbine cascades and stages. Computers & fluids, 33(5-6), 729-740.

[11] Ni, R. H. (1982). A multiple-grid scheme for solving the Euler equations. AIAA journal, 20(11), 1565-1571.

[12] Ziggaf, M, et al. "The FVC scheme on unstructured meshes for the two-dimensional Shallow Water Equations." International Conference on Finite Volumes for Complex Applications. Springer, Cham, 2020.

[13] Karel, J. (2014). Simulation numrique de la propagation d'une dcharge dans un plasma sur maillage non stucturs adapts dynamiquement (Doctoral dissertation, Paris 13).

[14] Desveaux, V. (2013). Contribution l'approximation numrique des systmes hyperboliques (Doctoral dissertation, Universit de Nantes).

[15] https://www.grc.nasa.gov/WWW/wind/valid/stube/stube.html

[16] https://github.com/pyccel/manapy